Letter Vol. 50, No. 16/15 August 2025/Optics Letters 4994

Integration of coherent spins in 4H-SiC beam splitters

Chengying Liu,[1,†] Yao Zhang,[1,†] Ailun Yi,[2,3,†] Qi Luo,[1] Yingjie Li,[1,4] Haibo Hu,[1,4] Tongyuan Bao,[1] Shumin Xiao,[1,4,5,6] Xin Ou,[2,3,7] Yu Zhou,[1,5,*] and Qinghai Song[1,4,5,6,8]

[1]Ministry of Industry and Information Technology Key Lab of Micro-Nano Optoelectronic Information System, Guangdong Provincial Key Laboratory of Semiconductor Optoelectronic Materials and Intelligent Photonic Systems, Harbin Institute of Technology, Shenzhen 518055, China
[2]State Key Laboratory of Functional Materials for Informatics, Shanghai Institute of Microsystem and Information Technology, Chinese Academy of Sciences, Shanghai 200050, China
[3]The Center of Materials Science and Optoelectronics Engineering, University of Chinese Academy of Sciences, Beijing 100049, China
[4]Pengcheng Laboratory, Shenzhen 518055, China
[5]Quantum Science Center of Guangdong-Hong Kong-Macao Greater Bay Area (Guangdong), Shenzhen 518045, China
[6]Collaborative Innovation Center of Extreme Optics, Shanxi University, Taiyuan 030006, Shanxi, China
[7]ouxin@mail.sim.ac.cn
[8]qinghai.song@hit.edu.cn
[†]These authors contributed equally to this work.
*zhouyu2022@hit.edu.cn

Received 14 May 2025; revised 25 June 2025; accepted 26 June 2025; posted 26 June 2025; published 7 August 2025

The SiCOI (silicon-carbide-on-insulator) platform is a promising solution for integrated quantum photonics. It offers excellent spin-photon interfaces and is compatible with CMOS fabrication processes. Beam splitters are essential in quantum optics, enabling critical operations such as quantum interference and entanglement generation. Most existing spin-integrated beam splitters rely on hybrid integration, where the quantum emitter and beam splitter are made from different materials, leading to efficiency losses. In contrast, SiCOI offers a unique opportunity for monolithic integration, where both the quantum emitter and the photonic device are made from the same material. However, despite the rapid advancements in SiCOI for photonic integration, spin-integrated beam splitters on this platform have yet to be realized. In this work, we demonstrate the integration of divacancy spin defects into SiCOI-based beam splitters, approaching a near 1:1 splitting ratio by tuning the coupling length (Lc). Using photoluminescence (PL) and optically detected magnetic resonance (ODMR) measurements, we confirm the successful integration and coherent control of the spin defects. These results provide initial steps for SiCOI-based quantum photonic circuits, paving the way for future scalable quantum photonic applications.

https://doi.org/10.1364/OL.567850

Introduction. The SiCOI (silicon-carbide-on-insulator) platform has emerged as a pivotal advancement in the field of integrated quantum photonics, attracting considerable attention due to its exceptional spin-photon interface properties [1,2] and compatibility with established CMOS fabrication techniques [3–6]. Over the past decade, silicon carbide (SiC), particularly the 4H-SiC polytype, has been recognized as an ideal material for quantum technologies, owing to its broad optical transparency from ultraviolet to infrared [7] and its ability to host stable quantum emitters [7] and spin defects [8–10]. These properties make SiCOI a promising platform for inteGrating quantum defects with photonic circuits, offering significant advantages, including outstanding optical properties [5,9,11,12], long spin coherence time [13,14], and the scalability of integrated photonics [3,15–17].

Beam splitters are essential components in quantum optics, enabling crucial operations such as quantum interference [18–23], quantum key distribution [24], and photonic entanglement generation [25–29]. Various methods have been developed to incorporate beam splitters into quantum photonic systems, including one-to-two splitters [30] and multimode interferometer (MMI) devices [31]. As the demand for scalable quantum photonic devices grows, hybrid integration presents a strategy to combine complementary technologies, such as CMOS-compatible photonics and quantum emitters (e.g., quantum dots or color centers), facilitating the creation of efficient and scalable photonic quantum circuits [30–34]. Hybrid integration enables unprecedented specialization of components, allowing the combination of the best aspects of various material platforms to create superior systems while maintaining excellent efficiency [35]. Its implementation requires careful management of interfacial losses. Another approach is monolithic integration [33,36,37], where the quantum emitter and the photonic device are produced from the same material. The SiCOI platform offers an ideal path for such integration. Despite rapid advancements in photonic integration on SiCOI [3,15], developing spin-integrated beam splitters remains challenging.

In this study, we address the challenge by demonstrating the integration of PL4 spin ensemble defects coupled into beam splitters on the SiCOI platform. These spin defects are introduced into the 4H-SiC membrane through ion implantation, and a near 1:1 splitting ratio is approached by tuning the coupling distance (Lc). The properties of the integrated photons and spin defects are characterized using photoluminescence (PL) spectroscopy and optically detected magnetic resonance (ODMR). This study provides a foundation for future work on scalable quantum photonic circuits, though additional research is required to refine the fabrication processes and ensure consistent performance.

Design and fabrication of the beam splitter. As shown in Fig. 1(a), the designed beam splitter consists of two primary components: the coupling area, which uses evanescent wave coupling to control energy exchange and achieve directional splitting, and two directional couplers to collect the emitted light through the objective. The geometry of the SiCOI beam splitter is designed to support only lower-order modes. The figure labels two key parameters: coupling length (Lc) and gap. To investigate the splitting ratio, the SiC waveguide width is fixed at 500 nm and height at 200 nm, while the coupling length is varied from 20 μm to 25 μm, and the gap from 90 nm to 110 nm. Adjusting these parameters achieves a 1:1 splitting ratio, as shown in Fig. 1(b), derived from FDTD (Finite-Difference Time-Domain using Lumerical) simulations. Within this parameter range, the splitting ratio varies from 0.08 to 8.06, with the dashed line representing the parameter combination for a splitting ratio of 1.0. A set of parameters was selected from Fig. 1(b) for simulation. The 50:50 splitting ratio in Fig. 1(b) arises from evanescent coupling between adjacent waveguides. The gap width governs the coupling strength: narrower gaps enhance the overlap of evanescent fields, accelerating periodic energy transfer between waveguides. Simultaneously, the device length determines the cumulative phase of this coupling process. Equal splitting occurs when light propagates half the coupling length required for complete energy transfer. The ideal parameters for a 50:50 split are marked with a dashed line, where a point Lc is 23.8 μm, the gap is 100 nm, and the inner diameter of a semicircular ring is 1.1 μm. The dimensions of the structure under this set of parameters are well-matched with the limits of the fabrication equipment and detection instruments, and the result is depicted in Fig. 1(c), showing the electric field distribution at the x-y cross-section when the power ratio at the output end of the beam splitter is 1.0. More details about the simulation can be found in Supplement 1.

Figure 2(a) illustrates the fabrication process of the 4H-SiC beam splitters. The process begins with the standard RCA cleaning of a 4-inch 4H-SiC wafer with an epitaxial layer. The wafer is bonded to an oxidized silicon substrate at room temperature under a pressure of 3000 N, followed by annealing at 800 °C for 6 hours to strengthen the bond. The grinding process reduces the SiC layer to approximately 3 μm. Chemical mechanical polishing (CMP) is then used to remove surface damage caused by grinding. The SiCOI wafer is diced into individual dies, and each die undergoes ICP dry etching to achieve the final thickness of 200 nm. Carbon ion implantation is performed with a dose of 10^{13} cm^{-2}. The beam splitters are fabricated by depositing a 30-nm Cr layer on the SiCOI membrane with ensemble spin. Different coupling lengths (Lc) are patterned onto ZEP 520 A electron-beam resist using electron-beam lithography with an overlay technique. After developing the resist, the Cr mask is formed through ICP dry etching. The SiC membrane is then etched to form the photonic devices, guided by the Cr hard mask, using ICP etching with 100 W RF and 1000 W ICP power at a pressure of 10 mTorr. More details of the fabrication can be found in Note 3 of Supplement 1. While the fabrication process showspotential, variability remains due to factors such as

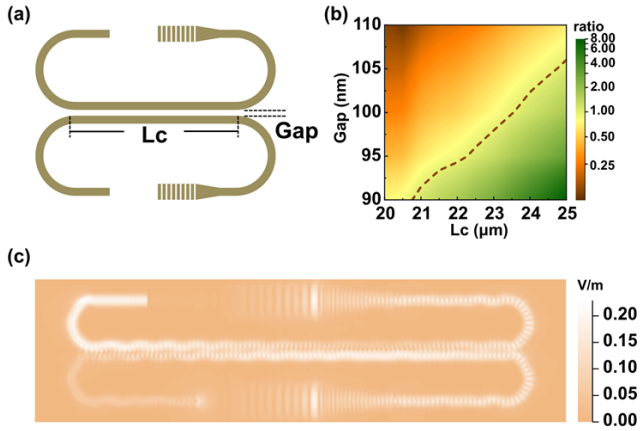

Fig. 1. Design of the 4H-SiCOI beam splitter. (a) Schematic of the SiCOI beam splitter, consisting of two main parts: the coupling area and the directional couplers for emission collection. The key parameters labeled are the coupling length (Lc) and the gap. (b) FDTD simulation results show the splitting ratio as a function of the coupling length (Lc) and gap. The dashed line indicates the parameter combination where the splitting ratio equals 1.0. (c) Electric field distribution at the x-y cross-section when the power ratio at the output end of the beam splitter is 1.0, determined by the coupling length and gap.

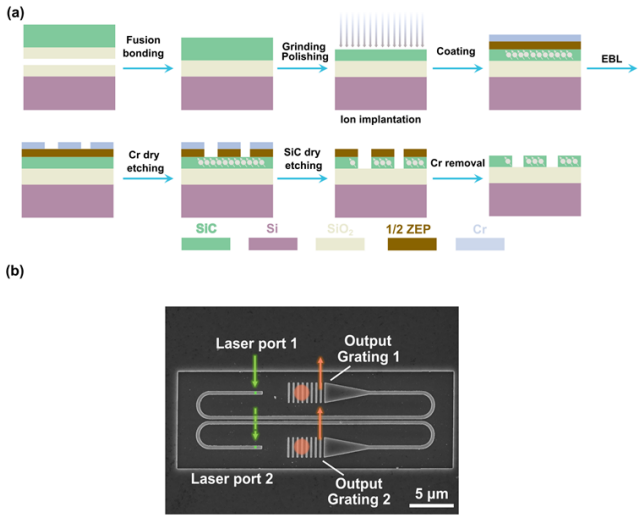

Fig. 2. Fabrication of the SiCOI beam splitter. (a) Flowchart of the fabrication steps for the SiCOI beam splitter, including cleaning, bonding, grinding, polishing, etching, and carbon ion implantation. (b) Scanning electron microscope (SEM) image of the fabricated SiCOI beam splitter. The green downward arrows represent the laser input ports (Laser Port 1 and Laser Port 2), and the red upward arrows indicate the output ports (Output Grating 1 and Output Grating 2). Non-confocal collection is achieved by using a scanning mirror in the collection arm.

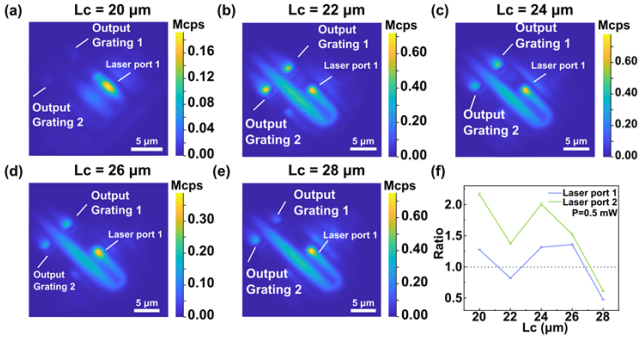

Fig. 3. Optical characterization of the SiCOI beam splitters. (a)–(e) Scanning images of the beam splitters, the excitation spot with 0.5 mW 914 nm laser is fixed at Laser Port 1 while the angle of the mirror is scanning, with coupling lengths of 20 μm, 22 μm, 24 μm, 26 μm, and 28 μm, showing distinct bright spots at both output ends. (f) The splitting ratio of the beam splitters with different coupling lengths is calculated by dividing the output from Grating 1 by that from Grating 2. The green and purple lines represent the splitting ratios for the two sets of outputs. The dashed line indicates the ideal 1:1 splitting ratio. The estimation of the coupling efficiencies and losses of the coupler is summarized in Note 4 of Supplement 1.

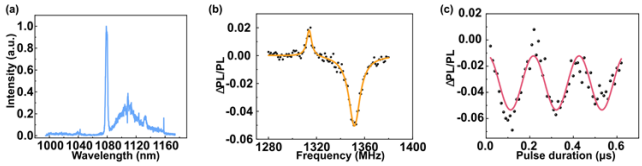

Fig. 4. Coherent control and characterization of spin defects in the beam splitter. (a) Photoluminescence spectrum showing the zero-phonon line (ZPL) at 1078 nm, confirming the presence of PL4 spin defects in the beam splitter. (b) ODMR measurements of the beam splitter integrated with PL4 defects showed resonance peaks at 1316 MHz with positive PL change and 1353 MHz with negative PL change. (c) Coherent control over the spin defects in the beam splitter, confirming the preservation of spin properties during fabrication.

mask roughness and internal reflections. Further optimization is necessary to enhance reproducibility and scalability.

The resulting fabricated beam splitter is shown in Fig. 2(b), where the green downward arrows represent the laser input ports (Laser Port 1 and Laser Port 2). The red upward arrows represent the collection ports (Output Grating 1 and Output Grating 2). Non-confocal collection is achieved by inteGrating a scanning mirror into the collection arm.

Optical characterization. Beam splitters with coupling lengths of 20 μm, 22 μm, 24 μm, 26 μm, and 28 μm were fabricated. A continuous-wave laser with a wavelength of 914 nm (0.5 mW) was used for excitation, and the sample was housed in a closed-cycle cryostat at 4 K. Laser Port 1 was excited. By scanning the angle of the mirror in the collection arm, the transmitted emission through the beam splitter was measured, as shown in Figs. 3(a)–3(e), for the different coupling lengths (Lc). Each device exhibits distinct bright spots at both output ends. In most cases, significantly less emission is observed on the same side as the excitation, indicating that the collected fluorescence is effectively coupled and transmitted through the directional couplers to the opposite waveguide. However, in some structures, a portion of the fluorescence is coupled back, resulting in a brighter emission on the same side as the excitation. This demonstrates the efficient coupling and transmission of fluorescence from the silicon carbide (SiC) ensembles within the beam splitter.

Additionally, comparing the five images reveals significant differences in the splitting ratios of the devices with varying coupling lengths. Specifically, the beam splitters with coupling lengths of 22 μm and 28 μm exhibit more photons emitted from Grating 2, while others show different output characteristics. This suggests that the coupling length (Lc) influences the output positions of the different modes formed in the waveguide during the evanescent wave coupling process, which in turn leads to varying splitting ratios. The splitting ratios (Grating 1/Grating 2) from both ends of the beam splitters were analyzed and are shown in Fig. 3(f). The ratios were calculated by dividing the output from the same side of the excitation port (Grating 1) by that from the opposite side (Grating 2). The green and purple lines represent the two sets of splitting ratios obtained from each end of the devices. The data trends are consistent, as the excitation and collection methods are symmetric. A dashed line indicates the 1:1 splitting ratio. These results suggest that the splitting ratio can be influenced by adjusting the coupling length (Lc), with the potential for improved ratio control under optimized fabrication conditions.

Coherent control of the spin ensembles in the beam splitter. To verify the emission from spin defects in SiC, the photoluminescence (PL) from the directional coupler was directed into a spectrometer and measured, as shown in Fig. 4(a). The zero-phonon line (ZPL), located around 1078 nm, suggests that the predominant defects generated by ion implantation are PL4 ensembles [38–40]. The PL spectra of the input and output ends of devices with different coupling lengths are displayed in Note 2 of Supplement 1. The fluorescence was detected using a superconducting nanowire single-photon detector after passing through a dichroic mirror and a 1000-nm long-pass filter. For the measurements of ODMR, Rabi, and Ramsey, a synthesized signal generator produced the microwave signals, which were subsequently gated by a switch. After amplification, the microwave signals were delivered to a 20-μm-wide copper wire positioned above the sample's surface. The excitation laser was modulated via an acoustic-optic modulator. A pulse generator was used to generate the timing sequence for the synchronization and manipulation of the electrical signals controlling the laser, microwave, and counter. Figure 4(b) presents the optically detected magnetic resonance (ODMR) measurements of the beam splitter integrated with PL4 ensembles, showing resonance peaks around 1316 MHz (with a positive PL change) and 1353 MHz (with a negative PL change). We demonstrated coherent control of the PL4 spin ensembles integrated with the beam splitter by varying the microwave duration. To determine if the fabrication of the beam splitter alters the spin properties of the PL4 spins, we measured the T1 and T2* before and after the integration, as shown in Note 5 of Supplement 1. No obvious degradation of both T1 and T2* has been observed. These results indicate that the spin properties of the defects are effectively preserved during the fabrication process.

Conclusions. In this work, we successfully demonstrated the integration of PL4 spin defects into beam splitters on the SiCOI platform. By tuning the coupling length (Lc), we achieved a near 1:1 splitting ratio although some variability in performance

is observed due to fabrication imperfections. The effective coupling and transmission of fluorescence from the spin defect ensemble have been confirmed. Both photoluminescence (PL) and ODMR measurements confirmed the presence of PL4 ensembles, showing distinct spin transitions. Furthermore, we demonstrated coherent control over the PL4 spin ensembles integrated into the device. While the SiCOI platform shows great promise for quantum photonic devices, challenges remain in optimizing spin-photon interactions and scaling the devices for larger applications [3,4,8,41,42]. Future research should focus on enhancing coupling efficiency and refining fabrication techniques. This work lays a foundation for developing SiCOI-based quantum photonic circuits.

Funding. The Innovation Program for Quantum Science and Technology (2024ZD0302100); Key Technologies Research and Development Program (2021YFA1400802, 2022YFA1404601, 2023YFB2806700); National Natural Science Foundation of China (12304568, 62293521, 12074400, 62205363); Basic and Applied Basic Research Foundation of Guangdong Province (2022A1515110382); Shenzhen Fundamental Research Project (JCYJ20241202123903005, JCYJ20230807094408018); Guangdong Provincial Quantum Science Strategic Initiative (GDZX2403004, GDZX2303001, GDZX2306002, GDZX2200001, GDZX2406002); Young Elite Scientists Sponsorship Program by CAST; New Cornerstone Science Foundation through the XPLORER PRIZE; Shanghai Science and Technology Innovation Action Plan Program (22JC1403300); Chinese Academy of Sciences Project for Young Scientists in Basic Research (YSBR-69).

Acknowledgment. Y.Z. acknowledges the support from Young Elite Scientists Sponsorship Program by CAST, Q.S. acknowledges the support from New Cornerstone Science Foundation through the XPLORER PRIZE, A.Y. acknowledges the support from Shanghai Science and Technology Innovation Action Plan Program (Grant No. 22JC1403300).

Disclosures. The authors declare no conflicts of interest.

Data availability. Data underlying the results presented in this paper are not publicly available at this time but may be obtained from the authors upon reasonable request.

Supplemental document. See Supplement 1 for supporting content.

REFERENCES

1. S. E. Economou and P. Dev, Nanotechnology **27**, 504001 (2016).
2. R.-Z. Fang, X.-Y. Lai, T. Li, *et al.*, Phys. Rev. Lett. **132**, 160801 (2024).
3. J. Wang, F. Sciarrino, A. Laing, *et al.*, Nat. Photonics **14**, 273 (2020).
4. D. M. Lukin, M. A. Guidry, and J. Vučković, PRX Quantum **1**, 20102 (2020).
5. M. A. Guidry, D. M. Lukin, K. Y. Yang, *et al.*, Nat. Photonics **16**, 52 (2022).
6. D. M. Lukin, C. Dory, M. A. Guidry, *et al.*, Nat. Photonics **14**, 330 (2020).
7. J. Wang, Y. Zhou, Z. Wang, *et al.*, Nat. Commun. **9**, 1656 (2018).
8. S. Castelletto, A. Peruzzo, C. Bonato, *et al.*, ACS Photonics **9**, 1434 (2022).
9. J. Wang, Y. Zhou, Z. Wang, *et al.*, Nat. Commun. **9**, 4106 (2018).
10. C. Liu, H. Hu, Z. Liu, *et al.*, Photonics Res. **12**, 1696 (2024).
11. C. Wang, Z. Fang, A. Yi, *et al.*, Light Sci. Appl. **10**, 139 (2021).
12. C. Wang, C. Shen, A. Yi, *et al.*, Light Sci. Appl. **11**, 341 (2022).
13. D. J. Christle, A. L. Falk, P. Andrich, *et al.*, Nat. Mater. **14**, 160 (2015).
14. K. C. Miao, J. P. Blanton, C. P. Anderson, *et al.*, Science **369**, 1493 (2020).
15. A. Yi, C. Wang, L. Zhou, *et al.*, Appl. Phys. Rev. **9**, 031302 (2022).
16. H. Hu, Y. Zhou, A. Yi, *et al.*, Nat. Commun. **15**, 10256 (2024).
17. T. Bao, W. Zhang, A. Yi, *et al.*, ACS Photonics **17**, 2988 (2025).
18. B. Machielse, B. A. Roberson, T. Kim, *et al.*, Phys. Rev. X **9**, 31022 (2019).
19. E. B. Flagg, A. Muller, S. V. Polyakov, *et al.*, Phys. Rev. Lett. **104**, 137401 (2010).
20. J. W. Silverstone, D. Bonneau, K. Ohira, *et al.*, Nat. Photonics **8**, 104 (2014).
21. H. Bernien, L. Childress, L. Robledo, *et al.*, Phys. Rev. Lett. **108**, 043604 (2012).
22. V. Giesz, S. L. Portalupi, T. Grange, *et al.*, Phys. Rev. B **92**, 161302 (2015).
23. J.-H. Kim, T. Cai, C. J. K. Richardson, *et al.*, Optica **3**, 577 (2016).
24. V. Scarani, H. Bechmann-Pasquinucci, N. J. Cerf, *et al.*, Rev. Mod. Phys. **81**, 1301 (2009).
25. W. B. Gao, A. Imamoglu, H. Bernien, *et al.*, Nat. Photonics **9**, 363 (2015).
26. D. D. Awschalom, R. Hanson, J. Wrachtrup, *et al.*, Nat. Photonics **12**, 516 (2018).
27. S. L. N. Hermans, M. Pompili, H. K. C. Beukers, *et al.*, Nature **605**, 663 (2022).
28. N. Kalb, A. A. Reiserer, P. C. Humphreys, *et al.*, Science **356**, 928 (2017).
29. B. Hensen, H. Bernien, A. E. Dréau, *et al.*, Nature **526**, 682 (2015).
30. J.-H. Kim, S. Aghaeimeibodi, C. J. K. Richardson, *et al.*, Nano Lett. **17**, 7394 (2017).
31. Y. Zhu, W. Wei, A. Yi, *et al.*, Laser Photonics Rev. **16**, 2200172 (2022).
32. J.-H. Kim, S. Aghaeimeibodi, J. Carolan, *et al.*, Optica **7**, 291 (2020).
33. R. Uppu, H. T. Eriksen, H. Thyrrestrup, *et al.*, Nat. Commun. **11**, 3782 (2020).
34. S. Chakravarthi, N. S. Yama, A. Abulnaga, *et al.*, Nano Lett. **23**, 3708 (2023).
35. N. H. Wan, T.-J. Lu, K. C. Chen, *et al.*, Nature **583**, 226 (2020).
36. C. Papon, X. Zhou, H. Thyrrestrup, *et al.*, Optica **6**, 524 (2019).
37. C. Papon, Y. Wang, R. Uppu, *et al.*, Phys. Rev. Appl. **19**, L061003 (2023).
38. A. L. Falk, B. B. Buckley, G. Calusine, *et al.*, Nat. Commun. **4**, 1819 (2013).
39. Q.-Y. Luo, Q. Li, J.-F. Wang, *et al.*, Front. Phys. **11**, 1270602 (2023).
40. W.-K. Quan, L. Liu, Q.-Y. Luo, *et al.*, Opt. Lett. **48**, 1423 (2023).
41. G. Moody, V. J. Sorger, D. J. Blumenthal, *et al.*, J. Phys. Photonics **4**, 012501 (2022).
42. M. Atatüre, D. Englund, N. Vamivakas, *et al.*, Nat. Rev. Mater. **3**, 38 (2018).